Simulation Bubble Nucleation and Bubble Growth of a Thermal-Bubble Microejector

Zhou Hongwei, A.M.Gué
Laboratoire d'Analyse et d'Architecture de systèmes (LAAS–CNRS), Université de Toulouse, 7 Avenue du Colonel Roche, 31077 Toulouse Cedex, France

E-mail : think.zhou@gmail.com

Abstract: The present study investigates simulation model and droplet ejection performance of a thermal-bubble microejector. This model simulates the bubble nucleation and the bubble growth, to predict the droplet ejection process. Specificity, it is achieved by coupling an electric-thermal model and flow model with bubble dynamics equations. The model is validated by comparing prediction results with experimental data. Moreover, the nucleation mechanisms, nucleation temperature and nucleation rate also are studied.

Keywords: microejector, thermal-bubble model, bubble nucleation, bubble growth, droplet volume and speed

1. Introduction

Depositing nanovolume of chemical or biochemical species with high precision and high reliability is today of major interest in various fields of applications. The functionalization of DNA chips is certainly the most challenging one. During the last ten years, many studies have been devoted to the development of miniaturize systems enabling the ejection of small droplet but most of them suffer from a lack of flexibility due to the difficulty to integrate high density arrays of individually addressable ejectors.

Thermal ejection is a good candidate to achieve simultaneously high density integration and individual actuation. This paper proposes a thermal ejection microarray [1] enabling in-situ oligonucleotide synthesis on DNA chips. It consists in a micro-array of individually addressable ejectors which eject nucleotides on a glass slide. The microejector is fabricated using monolithical silicon technologies. The microejector consists of three main elements, which are the supporting membrane, the resistance heater with the diode matrices for addressing and the SU8 nozzle.

The working principle of the microejector is based on a thermal-bubble inkjet printing [2-8]. A very short electric pulse is applied to a resistive heater to generate a high heat flux. If the surface temperature of the liquid is higher than the nucleation temperature, a vapor bubble is formed at the surface of the passivation layer. Sudden formation of the vapor bubble generates a pressure impulse, the rapid growth of the bubble expels a small liquid drop from the nozzle exit. After the applied current is removed, the temperature and pressure of the vapor decrease quickly, once the bubble collapses, the nozzle refills due to capillary forces for the next ejecting.

The operating cycle of a thermal-bubble microejector is shown in Figure 1. The operating cycle is divided into three phase: 1) the liquid is heated until bubble nucleation. 2) the bubble growth and collapse with droplet ejection. 3) refill of the reservoir.

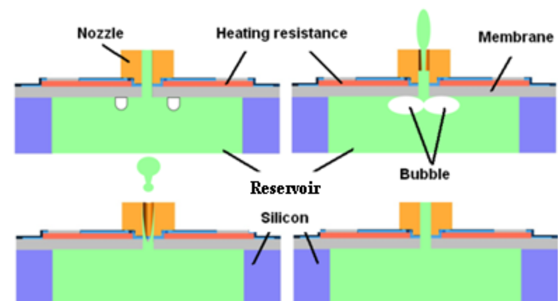

Figure 1: Schematic representation of the operating cycle, phase 1: bubble nucleation, phase 2: bubble growth and collapse with droplet ejection, phase 3: refill of the reservoir.

Three main problems should be resolved in designing thermal-bubble jet: bubble nucleation condition (temperature), the nucleation mechanism and ejection performance including the elimination of satellite droplets [13].

The nucleation mechanism [1, 9, 12] and the nucleation temperature [9-12] have been studied by a number of researchers. They suggest that the homogeneous nucleation is the primary mechanism for bubble nucleation in a thermal-bubble jet. The nucleation temperature increases as the heat rate increases.

In this paper, we present a thermal-bubble model to predict the droplet ejection process of the microejector, the method is based on the phase field formulation [8]. The droplet ejection performance is studied by performing numerical simulation using COMSOL Multiphysics.

2. Theory and method

The physical behavior of a heating flow is driven by the interface dynamics. The simulation model is achieved by coupling an electric-thermal model and flow model with bubble dynamics equations. The electric-thermal model deals with the heat transfer process in the liquid and solid. The fluid dynamic behavior of drop ejection in an incompressible, Newtonian fluid is governed by the Navier-Stokes equations. Bubble dynamics theory is used to simulate the nucleation and growth of the vapor bubbles. The bubble interface dynamics of a two-phase flow are governed by the Cahn-Hilliard equation.

2.1 Electric-thermal model

A heat transfer model is used for calculating the temperature distribution in liquid and solid before the bubble is generated. The governing equation of transient heat transfer with inner heat source is

$$\rho C_p \frac{\partial T}{\partial t} + \nabla \cdot (-k\nabla T) = Q_{dc} \quad (1)$$

where T is temperature, ρ density, C_p heat capacity, k thermal conductivity, Q_{dc} the heat input to the heater per unit volume per unit time.

2.2 Flow model

The liquid velocity field in the reservoir and the droplet velocity field are described by the incompressible Navier-Stokes equations:

$$\rho \frac{\partial u}{\partial t} + \rho u \nabla \cdot (u) = \nabla \cdot [-pI + \eta_L(\nabla u + (\nabla u)^T)] + \rho g \quad (2)$$

$$\nabla \cdot u = 0$$

where ρ is the fluid density, u the fluid velocity, p pressure, μ the viscosity, g gravity.

2.3 Bubble dynamics

It is observed that nucleation bubble instantaneously covers the surface of the heater in ~0.01 μs [12], the vapor bubble pressure is estimated very high, which can reach ~12 MPa. Once the vapor is nucleated, the vapor pressure is calculated by the Clausius-Clapeyron equation,

$$P_{sat} = P_{amb} exp[\frac{L}{k_B}\left(\frac{1}{T_b} - \frac{1}{T}\right)] \quad (3)$$

where P_{sat} is the saturated bubble pressure, L the latent heat of the liquid, T_b the boiling temperature of the liquid at ambient pressure, k_B the Boltzmann constant. The ideal gas law is expressed as

$$P_{sat}V = nK_bT$$

where V is the volume, n the number of moles of gas. The mass flux leaving the liquid surface leads to an increase in pressure of the vapor. The pressure exerts a force on the liquid surface and the vapor region begins to expand. The mass flux can be evaluated from the conductive heat flux, which can be approximated by the following expression:

$$\dot{m} = -\left(\frac{M_w}{\Delta H_{vl}}\right) n \cdot K_v \nabla T_v \approx C\rho_L \frac{(T-T_{sat})}{T_{sat}} \quad (4)$$

where M_w is the molecular weight of the vapor, ΔH_{vl} is the enthalpy of vaporization and C is a constant (m/s). The mass flux is generated by the bubble growth. So, the mass flux appears in the energy equation (1) as:

$$\rho C \frac{\partial T}{\partial t} + \rho C_p (u \cdot \nabla)T = -\nabla \cdot (-k\nabla T) - \left(\frac{\dot{m}\delta \Delta H_{vl}}{M_w}\right) \quad (5)$$

2.4 Phase Field Method

The bubble interface is tracked using the volume of fluid (VOF) technique. The equations governing the interface dynamics of a two-phase flow can be described by the Cahn-Hilliard equation. The equation for the phase field variable is modified to allow for the change of phase:

$$\frac{\partial \emptyset}{\partial t} + u \cdot \nabla \emptyset - \dot{m}\delta\left(\frac{V_{f,V}}{\rho_V} + \frac{V_{f,L}}{\rho_L}\right) = \nabla \cdot \frac{\gamma\lambda}{\varepsilon^2} \nabla \psi \quad (6)$$

where $\emptyset$ is the dimensionless phase field variable such that $-1 \le \emptyset \le 1$. The quantity λ is the mixing energy density (N) and ε is a capillary width that scales with the thickness of the interface (m). Therefore, over the interface, a volume fraction is defined as

$$V_f = \frac{1 + \emptyset}{2}$$

The volume fraction of the vapor and liquid phase are $V_{f,v} \in$[-1,0] and $V_{f,L} \in$ [0,1], repectively. The two parameters of the quantity λ and the capillary width ε are related to the surface tension coefficient via:

$$\sigma = \frac{2\sqrt{2}}{3}\frac{\lambda}{\varepsilon}$$

and γ is the mobility. The mobility determines the time scale of the Cahn-Hilliard diffusion. The default value, $\gamma = \varepsilon^2$, is usually a good initial guess. The equation governing ψ is:

$$\psi = -\nabla \cdot \varepsilon^2 \nabla \emptyset + (\phi^2 - 1)\phi$$

The quantity, δ is a smoothed representation of the interface between the two phases. It is defined as:

$$\delta = 6V_f(1 - V_f)\frac{|\nabla\phi|}{2}$$

The continuity equation is modified to account for the phase change from liquid to vapor:

$$\nabla \cdot u = \dot{m}\delta\left(\frac{1}{\rho_V} - \frac{1}{\rho_L}\right) \quad (7)$$

2.5 Physical Properties

The thermal conductivity and specific heat capacity are computed as functions of the volume fraction of the two phases:

$$k = (k_L - k_v)V_{f,L} + k_v \quad (8)$$

$$C_p = (C_{p,L} - C_{p,v})V_{f,L} + C_{p,v} \quad (9)$$

The simulation tool solves equations (1)–(9) with appropriate boundary conditions, to simulate bubble nucleation and bubble growth.

2.6 Simulation method

The simulation process is divided into two stages: In phase 1, before the bubble is nucleated, the liquid is treated as a solid. An electric-thermal model deals with the heat transfer process. In phase 2, after the bubble is nucleated, the bubble growth with liquid motion is solved by coupling flow and energy with the bubble dynamics equations. Heat, mass and momentum transfers with a phase-change process are also considered in bubble growth model.

3. Simulation

3.1 Description of the device structure

The microejector head is presented in Figure 3, which was integrated on a dielectric and stress free membrane [14]. The membrane was obtained by stacking a thermal silicon dioxide layer (1.4 µm thick) and a LPCVD $SiN_{1.2}$ layer (0.6 µm thick). The heating element was an annular resistance made of doped LPCVD polysilicon (0.5 µm thick) and encircling symmetrically the ejection hole.

The polysilicon heaters were insulated from upper layers by a PECVD SiO_2 film. The connecting part was heavy doped by diffusion. The inner and external radius of the heater is 60 µm and 80 µm, respectively. Two levels of connecting tracks realized by Ti/Au sputtering were separated by a SiO_2 layer.

Ejector nozzles have been realized by patterning a SU-8 40µm thick layer [15], ICP-DRIE etching achieved the reservoir by etching the silicon wafer from the back side. The reservoir was closed by assembling the micro-array with another silicon wafer, which was used for connecting the tube, and finally, the chips were mounted onto a Printed Circuit Board to facilitate using.

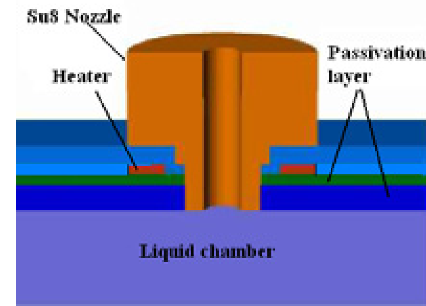

Figure 3: A cross-sectional view of the microejector

3.2 Description of the computational model

A schematic diagram of the computational model of the microejector is presented in Figure 2. The heater width is w and the thickness of the heater is 0.5 µm. The water in the reservoir is of density ρ_{water}, viscosity μ_{water} and surface tension σ, the air outside the nozzle is of density ρ_{air}, viscosity is $\mu_{air.}$ The heat capacity of water is Cp_l, and the heat capacity of air is Cp_g. The thermal conductivity of the water is k_l. The glass slide is located at a distance of 0.35 mm from the nozzle

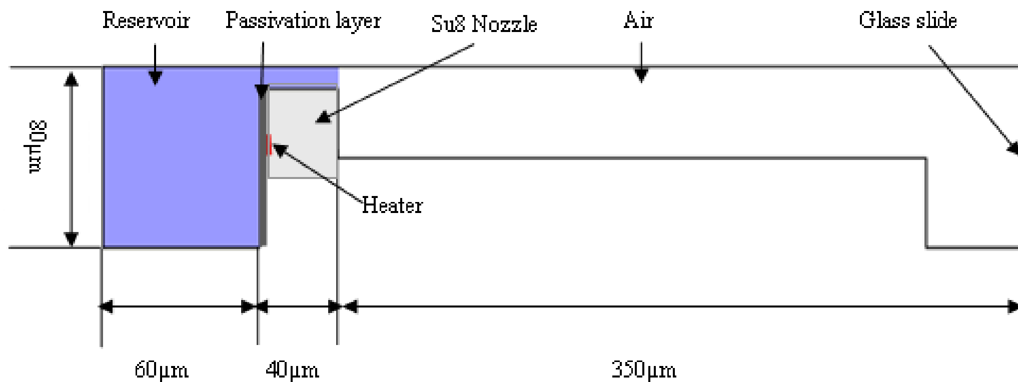

Figure 2: Computational model of the microejector

orifice. The width of the thermal pulse applied to the heater element is τ.

3.3 Boundary conditions and the constant parameters

The geometry of the microejector is axial-symmetric, so an axisymmetric two-dimensional model was used for simulating the microejector in order to reduce the calculation time. The boundary conditions for the models are illustrated with reference to Figure 4.

In electric-thermal model, boundary 5-1 is inward current boundary, and boundary 5-2 is electric ground. Others boundaries are electric insulation boundaries. In flow model, boundary 1 is symmetry boundary condition, boundary 2 is the inlet boundary and the fluid fraction function $\emptyset = 1$, boundary 3 is the slip boundary which indicates that the droplets slips at the glass slide, boundary 10 is the outlet boundary, the pressure is 101325 Pa. All the solid boundaries are no-slip boundaries. The initial temperature in the computational domain is 300 K. The conductivity of the heating resistance is 2300 S m^{-1}.

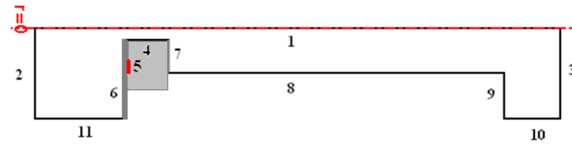

Figure 4: Boundaries of computational domain

The materials properties used for the microejector is listed in Table 1.

Table 1: Properties of the materials

Material	K(W/m·K)	ρ(kg/m^3)	C_p (J/Kg·K)
Silicon	100	2328	702
Polysilicon	100	2328	700
SiO_2	1.4	2070	840
SiN_X	1.67	3200	714
SU8	0.2	1190	1200
Water	0.614	1000	4180

3.4 The dimension of the microejector geometry

The geometry of the model is depicted in Figure 2, and has the following dimensions: the height of the nozzle is 40 µm and the radius of the nozzle is 10 µm. The height, width of the heater is 0.5 µm and 10 µm, respectively, and the inner radius of the heater is 30 µm. The height of reservoir is 60 µm and the radius diameter of reservoir is 80 µm.

4. Simulation results

4.1 Temperature distribution

Time evolution of the vapor profile with the temperature contours in the liquid is shown in Figure 6, when the applied current is 20 mA with a pulse duration of 5 µs. The surface temperature between the liquid and the passivation layer increases rapidly in 5 µs. However, the maximum surface temperature is 582 K at 7.5 µs due to the time required for heat transfer to take place through the passivation layer.

The deformation of temperature profile arises from the displacement of the liquid. It is observed that the thickness of the liquid region is less than 0.1 µm. This is why the water almost didn't burn out. It can help the bubble collapses.

4.2 Nucleation temperature

As shown in Figure 5 and Figure 6, the liquid begins to boil only when it is heated close to the superheat temperature [9-12] of 540 K at 6 µs.

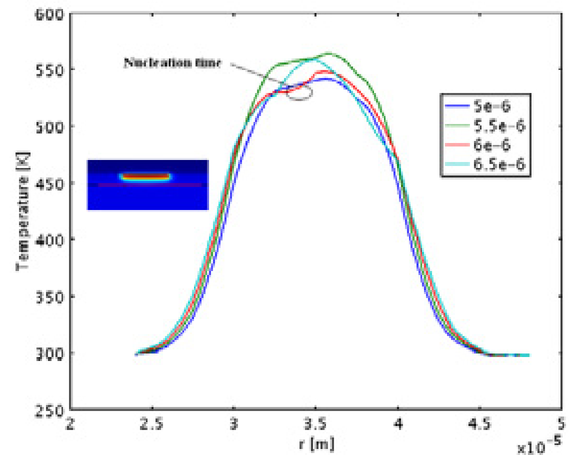

Figure 5: Temperature distribution of the water and vapor under the heater in r-axis direction at 5, 5.5, 6 and 6.5 µs.

4.3 Bubble dynamics

The growth of the vapor bubble expels a water drop is shown at 3 µs, 6 µs and 8µs in Figure 6. The bubble nucleation temperature is 540 K. The bubble is growing from 6µs to 8.5µs, and the maximum volume of vapor is 3.7 pL. However, the droplet volume is 1.9 pL. The average speed of the water droplet is calculated to be approximately 12.5 m s^{-1}.

Figure 6 shows the bubbles collapse process at 9.5 µs, 15 µs and 30 µs. The bubbles collapse as the temperature and the vapor pressure decrease after t = 8.5 µs, the long duration negative pressure in bubble induces the bubbles collapse. The fluid in the chamber is retracted toward the collapsing bubbles, the capillary force refills the fluid in the nozzle for the next ejection. The bubble collapse time is 16.5 µs.

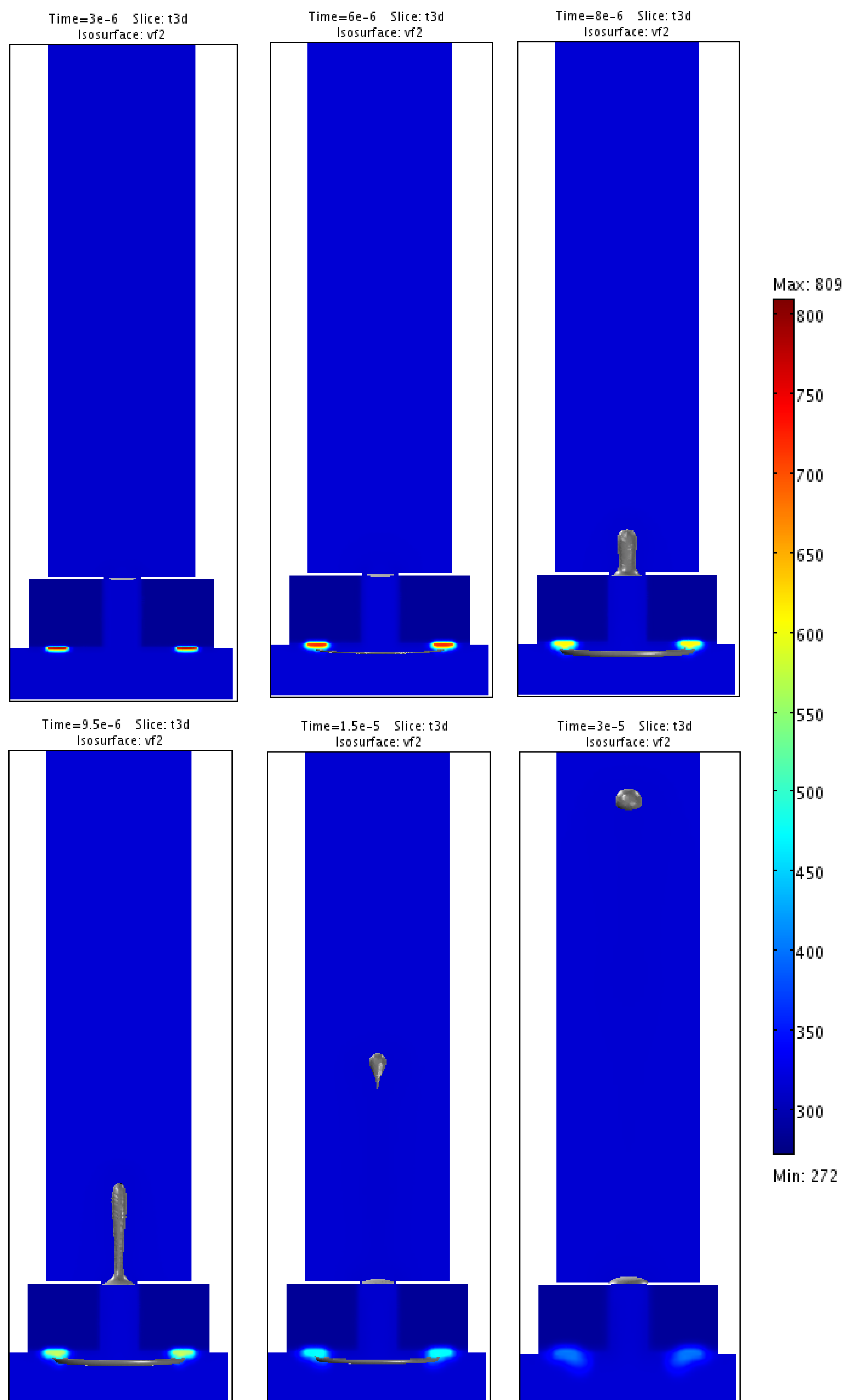

Figure 6: Time (s) evolution of the vapor profile with the temperature (K) contours in the liquid. The applied current is 20 mA with a pulse duration of 5 μs.

5. Experimental setup-up and the measurement results

The Schematic diagram of the experimental setup is described in Figure 7. The microejector was installed on the measurement system. Firstly, the power supply (Keithley 2410) was set as a current driven power, the current limit was 15 mA, and the voltage limit was 28 V. The pulse width was adjusted by a designed control circuit. Secondly, the led light source was opened, and the camera was focused on the nozzle of the chip to see the ejection droplet motion. Thirdly, the water was filled to the reservoir through the tube of the microejector. And finally, the operating current with pulse width was adjusted to an appropriate value for ejecting a droplet, which hit the target glass slide. The ejection place on the glass slide was changed by motion control system. The camera was focused on the glass slide to see the droplet dynamics clearly. The radius of the droplet was measured by the microscope.

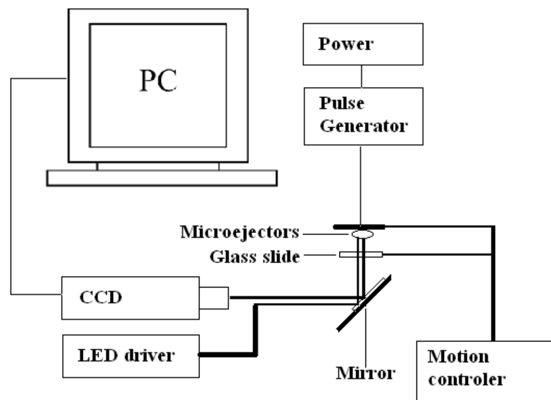

Figure 7: Schematic diagram of the experimental setup

The glass slide surface is located at a distance of 0.35 mm from the nozzle orifice. The properties of the buffer used for the experiment are as follows: density 1600 kg m^{-3}, viscosity 0.0015 Pa s and surface tension 0.08 N m^{-1}. The operating current is 3 mA with a pulse duration of 5 ms, the photograph of the ejected droplets is presented in Figure 8 (a), the radius of the bubble droplet is 24.5 μm. The radius droplet of simulation is 25.5 μm when the applied current is 3 mA with a pulse duration of 4.5ms (Figure 8 (b)). The present numerical results are compared with the experimental data, the difference is within 10%.

6. Conclusions

The present study investigates simulation model and droplet ejection performance of a thermal-bubble microejector. This model simulates the bubble nucleation and the bubble growth, to predict the droplet ejection process. Specificity, it is achieved by coupling an electric-thermal model and flow model with bubble dynamics equations. The model is validated by comparing prediction results with experimental data. For the optimization or the designing of a new thermal-bubble jet, this model provides a basic approach to investigate the effects of geometry or thermal energy on droplet volume and speed.

The typical working current and pulse width of the microejector are 14.5 mA, 10 µs, 20 mA, 5 µs and 24 mA, 3 µs, respectively. The droplet volume varies from 1 pL to 15 pL for the power consumption ranging from 45 mW to 0.4 W.

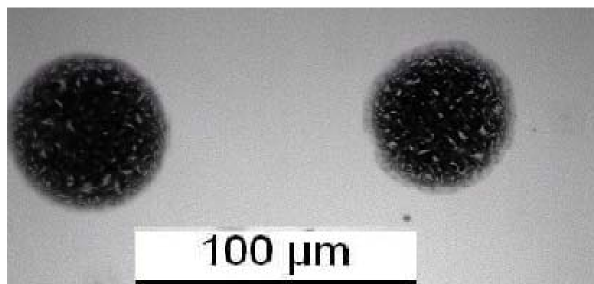

a)

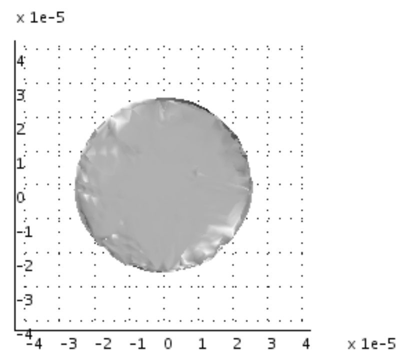

b)

Figure 8: (a) is the photograph of the ejected droplets on the glass slide, the radius of the droplet is 24.5 µm. b) is the droplet of simulation on glass, the radius of the droplet is 25.5 µm.

References

1. A.M. Gué, T. Phou, D. Jugieu and V. Conédéra, An ejection microarray for in-situ oligonucleotide synthesis on DNA chips, *Transducers'03 Boston*, USA, June 8–12, pp 218–21, 2003.
2. R. R. Allen, J. D. Meyer, and W. R. Knight, Thermodynamics and Hydrodynamics of Thermal Ink Jets, *Hewlett Packard J.*, vol. 36, pp. 21–27, 1985.
3. A. Asai, T. Hara, and I. Endo, One-Dimensional Model of Bubble Growth and Liquid Flow in Bubble Jet Printers, *Jpn. J. Appl. Phys.*, vol. 26, pp. 1794–1801, 1987.
4. A. Asai, Three-Dimensional Calculation of Bubble Growth and Drop Ejection in a Bubble Jet Printer, *J. Fluid Eng.*, vol. 114, pp. 638–641, 1992.
5. Y. Hong, N. Ashgriz, J. Andrews, and H. Parizi, Numerical Simulation of Growth and Collapse of a Bubble Induced by a Pulsed Microheater, *J. MEMS*, vol. 13, pp. 857–869, 2004.
6. A. K. Sen and J. Darabi, Droplet Ejection Performance of a Monolithic Thermal Inkjet Print Head, *J. Micromech. Microeng.*, vol. 17, pp. 1420–1427, 2007.
7. Y. Suh and G. Son, A Level-Set Method for Simulation of a Thermal Inkjet Process, *Numer. Heat Transfer B*, Vol. 54, pp. 138-156, 2008.
8. G. Son, A Numerical Method for Bubble Motion with Phase Change, *Numer. Heat Transfer B*, vol. 39, pp. 509–523, 2001.
9. C.T. Avedisian, W.S. Osborne, F.D. McLeod and C.M. Curley, Measuring bubble nucleation temperature on the surface of a rapidly heated thermal ink-jet heater immersed in a pool of water, *Proc. R. Soc. London*, A 455, pp. 3875–3899, 1999.
10. P.G. Deng, Y.-K. Lee and P. Cheng, Measurements of micro bubble nucleation temperatures in DNA solutions, *J. Micromech. Microeng.,* Vol. 15 , 564–574, 2005.
11. D M van den Broek and M Elwenspoek, Bubble nucleation in an explosive micro-bubble actuator, *J. Micromech. Microeng.,* vol.18, 064003 (8pp), 2008.
12. A. Asai, Application of the nucleation theory to the design of bubble jet printers, *Jpn. J. Appl. Phys.*, vol. 28, no. 5, pp. 909–915, 1989.
13. F.-G. Tseng, C.-J. Kim and C.-M. Ho, A high-resolution high-frequency monolithic top-shooting microinjector free of satellite drops. Part I. Concept, design, and model. *J. Microelectromech. Syst., vol.* 11**,** pp. 427–436, 2002.
14. Rossi, C. et al, Realization and performance of thin SiO_2/SiN_X membrane for micro-heater applications, *Sensors and Actuators A,* Vol. 64, pp. 241-245, 1998.
15. D. Jugieu, T. Phou, A.M. Gué, Technological development of a micro-array of individually addressable ejector, *Sensors and Actuators B*, Vol. 114, pp. 656-664, 2006.